

Direct Observation of Nitrogen Location in Molecular Beam Epitaxy Grown Nitrogen-Doped ZnO

P. Fons*, H. Tampo*, A. V. Kolobov*, M. Ohkubo*, S. Niki*, J. Tominaga*, R. Carboni[†] and S. Friedrich**

*National Institute of Advanced Industrial Science & Technology, Tsukuba Central 4, Higashi 1-1-1, Tsukuba, Ibaraki, 305-8562, Japan

[†]Physics Department and CNISM, University of Bologna, viale C. Berti Pichat 6/2, 40127 Bologna, Italy

**Advanced Detector Group, L-270 Lawrence Livermore National Laboratory, Livermore, CA 94550, U.S.A.

Abstract. ZnO is a wide band gap, naturally n-type semiconductor with great promise for optoelectronic applications. To date, however, it has proven difficult to dope p-type, a prerequisite for device fabrication. Nitrogen is widely believed to be one of the most promising dopant candidates, however, experimental results to date have been inconsistent; recent theoretical formation energy calculations have indicated that Nitrogen preferentially incorporates into the ZnO lattice in the form of a N_2^- molecule at an O-site when a Nitrogen plasma source is used, leading to compensation rather than p-type doping. We show by a combination of X-ray absorption spectroscopy at the N K-edge of plasma-assisted molecular beam epitaxy grown ZnO and ab-initio simulations that in as-grown material, Nitrogen incorporates substitutionally on an O-site where it is expected to act as an acceptor. We have also observed the distinctive formation of molecular nitrogen bubbles upon rapid thermal annealing. These results suggest that effective p-type doping of ZnO with N may only be possible for metastable low-temperature growth processes.

Keywords: ZnO, Nitrogen, doping, XAFS

PACS: 61.10Ht, 71.15MB, 68.55.Ln, 66.30.Jt

INTRODUCTION

Zinc Oxide (ZnO) has been the subject of renewed research over the past several years in large part to its similarities to GaN. Both crystallize in the wurtzite structure (P6₃mc) and have comparable lattice constants (GaN: $a=0.3189$, $c=0.5185$, ZnO: $a=0.3250$, $c=0.5207$ Å) and bandgaps (GaN: 3.36 eV, ZnO: 3.35 eV). ZnO, however, has several advantages not shared by GaN or its alloys including the facts that its constituents are plentiful and inexpensive, bulk substrates are available and it can be allowed with Mg to form the pseudobinary $Mg_xZn_{1-x}O$ alloy allowing the growth of single-phase alloys with bandgaps up to 4.0 eV.

Much of the utility of ZnO in optoelectronic or spintronic applications lies requires the fabrication of p-type material, a property that has proven to be elusive. Reports to date on the fabrication of p-type ZnO have not been reproduced by other groups and the lack of a broadly accepted technique for p-type doping is limiting the applications of ZnO. The combination of very low activation energy for n-type dopants, the existence of several dominant native defect and hydrogen related donor levels [1] located within 0.01-0.05 eV of the conduction band edge combined with the anticipated relatively high activation of p-type dopants leads to ambiguity in electrical results in the study of p-type doping due to strong

carrier compensation effects. Nitrogen is widely considered to be the most promising p-type dopant due to its similar size to oxygen, resistance to forming AX centers [2], and its successful use in other II-VI compounds such as ZnSe [3].

In situations such as the above, theoretical results can often provide insight. Recently, density functional theory (DFT) has been applied to determine the formation energy of various types of compensating defects for nitrogen-doped ZnO in the presence of a plasma source[4]. By using a value for the N chemical potential that took into account the presence of a mixture of ground and excited state N_2 in the doping flux, it was shown that the calculated N maximum solubility increased over eight orders of magnitude with the use of a plasma N source. Concomitant with the use of a plasma N source, it was also found that the N-related defect with the lowest formation energy was a N_2 defect at an O-site. The conclusion drawn was that compensation effects from the double donor N_2 defect would dominate and lead to electron-based conduction. Since these calculations depend strongly on the atomic chemical potentials and the fermi level and would seem to rule out the efficacy using Nitrogen as a p-type dopant, confirmation by experiment is desirable. To this end, we have applied soft x-ray absorption at the K-edge of N (403 eV) and first-principles real-space scattering simulations to

directly observe the location of N in the ZnO lattice both in as-grown and thermal annealed states.

EXPERIMENT

Although epitaxial ZnO has been grown by a variety of techniques including RF sputtering[5], MO-chemical vapor deposition[6], and laser-ablation[7] among others, we focus here on radical source-molecular beam epitaxy (RS-MBE)[8]. In RS-MBE, Zn flux is provided by an elemental (7N) effusion cell while O and N fluxes originate from RF-radical (gas) cells. Details of the growth procedure have been described previously [9]. The film growth temperature was fixed at 450° C for all samples; the sample thickness was approximately 1 μ m. Samples with a variety of N₂ flow rates with differing II/VI ratios were grown. For the as-grown samples, calibrated SIMS depth profiling measurements indicated a nearly constant N signal with average N concentrations approaching 1% ($9 \times 10^{20} \text{ cm}^{-3}$). This value may be compared with the electron densities $\lesssim 1 \times 10^{17} \text{ cm}^{-3}$ and $\lesssim 10^{12} \text{ cm}^{-3}$ for an undoped ZnO film and the hydrothermal ZnO substrates, respectively.

After growth, all samples were divided into two pieces: one half was retained as an as-grown standard, while the other half underwent rapid thermal annealing (RTA) to investigate thermal stability. All RTA samples were heated to 800° C for three minutes. It was noted that as-grown samples appeared transparent, but yellow in color, while the same samples after RTA treatment were perfectly transparent. Hall effect electrical measurements made using the Van der Pauw geometry revealed for a typical N-doped sample grown on the Zn face of a ZnO wafer, the initial carrier concentration was $\lesssim 5 \times 10^{15} \text{ cm}^{-3}$ ($\mu \sim 10 \text{ cm}^2/\text{Vs}$), rising to $\sim 6 \times 10^{17} \text{ cm}^{-3}$ ($\mu \sim 70 \text{ cm}^2/\text{Vs}$) after RTA processing.

The N-doped ZnO samples were measured at two locations the ELETTRA synchrotron in Trieste, Italy and the Advanced Light Source at Lawrence Berkeley National Laboratory. The ELETTRA measurements were carried out at beamline ALOISA. ALOISA is an undulator beamline with a photon flux of approximately 10^{11} photons/sec. The beam was linearly polarized and was incident upon the sample at approximately 50° degrees. X-ray fluorescence radiation was detected using a windowless single element Ge solid-state detector (SSD). The use of photon counting allowed measurement of samples from the high 10^{19} cm^{-3} concentration range. Due to the close proximity of the O K-edge ($\sim 540 \text{ eV}$), only near-edge ($\lesssim 100 \text{ eV}$) measurements at the N K-edge ($\sim 409 \text{ eV}$) were carried out. Crystals in the wurtzite structure have two distinct XANES patterns, one for polarization along the [001] axis and another

for polarization in-plane. For non-polarization dependent measurements, an incident angle of approximately 50° was used resulting in a weighted sum of the two possible polarization spectra; the sample geometry was taken into account for all simulations. Polarization-dependent measurements were taken using a novel multielement superconducting detector at beamline 4.0.2 (photon flux $\sim 10^{12}$ photons/second) of the Advanced Light Source at Lawrence Berkeley National Laboratory [10].

RESULTS AND DISCUSSION

XAFS measurements on an as-grown N-doped ZnO sample along with simulated results are shown in Fig.1. Data was interpreted using a two step process. Ground-state DFT calculations were used to relax the ZnO lattice around various N lattice positions and then these relaxed coordinates were used as input to a real-space, full multiple scattering simulation for comparison with experiment.

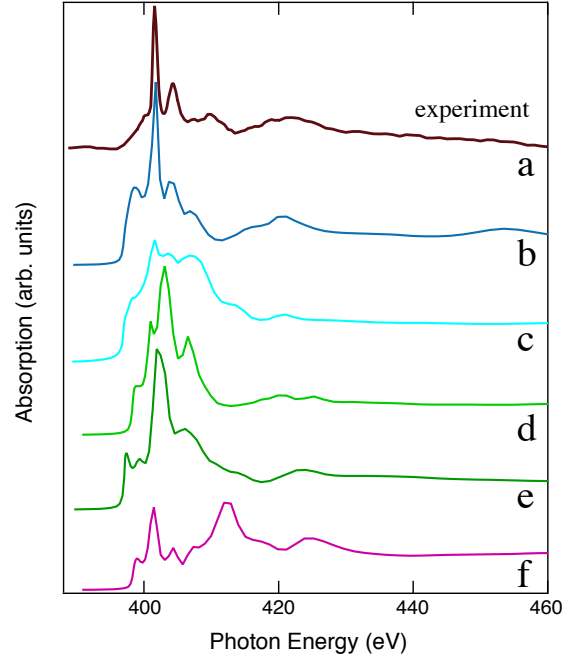


FIGURE 1. Experimental (a) and simulated real space multiple scattering XANES simulations for various DFT relaxed N local environments including (b) N on an O site, (c) N₂ on an O site, (d) N in a tetrahedral interstice, (e) N in a Zn site, and (f) N in an octahedral interstice. The energy step was 0.5 eV.

In the first step, an impurity N atom was placed at a high symmetry position in the ZnO lattice and the surrounding atoms were relaxed to their ground state positions using Broyden minimization. Potentials were calculated self-consistently using a conjugate-gradient algorithm[11]. The norm-conserving pseudopotentials in

the Troullier-Martins scheme used for the calculation included the $3d^{10}4s^2$ (Zn), $2s^22p^4$ (O), and $2s^22p^3$ (N) valence electrons as well as non-local core corrections. The generalized gradient approximation (GGA) as expressed by the Perdew-Burke-Ernzerhof exchange formulation was used [12]. Calculations were carried out on 32 atom supercells using a plane wave cutoff energy of 50 Hartree. The final atom positions as expressed by the relaxed supercell where embedded into a DFT relaxed ZnO spherical cluster and used as input to the ab-initio real space full multiple-scattering (FMS) code FEFF8 for the calculation of the simulated x-ray absorption spectra[13]. Studies of cluster size using FEFF8 demonstrated that convergence was reached for cluster sizes greater than 200 atoms, hence all results presented here are for clusters that size. Fig.1 shows the results of these calculations while an interpretation of these results is provided in the next section.

CONCLUSION

The DFT calculations in general showed significant lattice relaxation for Nitrogen locations other than on the O-site resulting in peak broadening and a significant discrepancy from experiment. The simulated spectra for Nitrogen incorporating on an O site showed excellent agreement with experiment. After annealing, the samples showed only a single peak. A more detailed examination of both the as-grown and annealed samples was carried out at beamline 4.0.2 at the ALS; this data can be seen in Fig.2. The annealed spectra are an excellent match to the characteristic spectra of the molecular vibration levels of a N_2 molecule. In addition, as the spectra show no polarization dependence, it is strongly suggested that the Nitrogen contained in the films has transformed to N_2 , presumably in the form of bubbles. This behavior is also consistent with the change in sample color from yellow to transparent as N moves from electronically active sites to electronically inactive bubbles. In contrast, no such fine structure is visible in the as-grown film seen in Fig.2(e).

ACKNOWLEDGMENTS

The DFT results were obtained through the use of the ABINIT code, a common project of the Université Catholique de Louvain, Corning Incorporated, and other contributors (URL <http://www.abinit.org>). We are also grateful to the ALOISA staff for help with the experiment. Measurements at ELETTRA were supported by the Synchrotron Radiation Committee of Istituto Nazionale per la Fisica della Materia. S.F. acknowledges NSF, DOE OBER and NA-22 funding. Part of this work was performed under the auspices of the U.S. Depart-

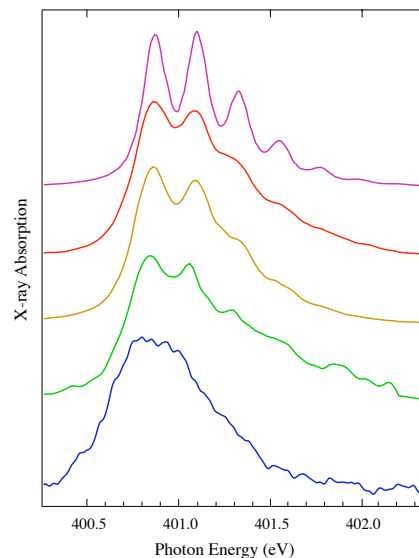


FIGURE 2. Polarization measurements made for (a) a molecular N_2 gas standard and on a N-doped ZnO sample after annealing for \mathbf{E} (b) along the c-axis, (c) at 45° to the c-axis, (d) in the a-b plane. (e) shows the equivalent range for an as-grown sample. The energy step was 40 meV

ment of Energy by Lawrence Livermore National Laboratory under contract No. W-7405-ENG-48.

REFERENCES

1. C. Van de Walle, *Phys. Rev. Lett.* **85**, 1012–1015 (2000).
2. C. H. Park, S. B. Zhang, and S.-H. Wei, *Phys. Rev. B* **66**, 073202 (2002).
3. K. Ohkawa, T. Karasawa, and T. Mitsuyu, *J. Cryst. Growth* **111**, 797–801 (1991).
4. E. Lee, Y. Kim, Y. Jin, and K. Chang, *Physica B* **308**, 912–915 (2001).
5. Y. Igasaki, and H. Saito, *J. Appl. Phys.* **69**, 2190–2195 (1991).
6. Y. Liu, C. Gorla, S. Liang, N. Emanetoglu, Y. Lu, H. Shen, and M. Wraback, *Journal of Electronic Materials* **29**, 69–74 (2000).
7. S. Choopun, R. Vispute, W. Noch, A. Balsamo, R. Sharma, T. Venkatesan, A. Iliadis, and D. Look, *Appl. Phys. Lett.* **75**, 3947–3949 (1999).
8. P. Fons, K. Iwata, A. Yamada, K. Matsubara, and S. Niki, *J. Crystal Growth* **201-202**, 627 (1999).
9. P. Fons, K. Iwata, A. Yamada, K. Matsubara, K. Nakahara, T. Tanabe, H. Takasu, and S. Niki, *Appl. Phys. Lett.* **12**, 1801–1803 (2000).
10. S. Friedrich, T. Funk, O. Drury, S. Labov, and S. Cramer, *Rev. Sci. Instr.* **73**, 1629–1631 (2002).
11. X. Gonze, *Phys. Rev. B* **54**, 4383 (1996).
12. J. Perdew, K. Burke, and M. Ernzerhof, *Phys. Rev. Lett.* **77**, 3865–3868 (1996).
13. A. Ankudinov, and J. Rehr, *Phys. Rev. B* **62**, 2437 (2000).